Phase-noise measurements in long-fiber interferometers for quantum-repeater applications

Jiří Minář, Hugues de Riedmatten, Christoph Simon, Hugo Zbinden, and Nicolas Gisin
Group of Applied Physics, University of Geneva, CH-Geneva, Switzerland
(Received 29 November 2007; published 20 May 2008)

Many protocols for long distance quantum communication require interferometric phase stability over long distances of optical fibers. In this paper we investigate the phase noise in long optical fibers both in laboratory environment and in installed commercial fibers in an urban environment over short time scales (up to hundreds of μs). We show that the phase fluctuations during the travel time of optical pulses in long-fiber loops are small enough to obtain high visibility first-order interference fringes in a Sagnac interferometer configuration for fiber lengths up to 75 km. We also measure phase fluctuations in a Mach-Zehnder interferometer in installed fibers with arm length 36.5 km. We verify that the phase noise respects Gaussian distribution and measure the mean phase change as a function of time difference. The typical time needed for a mean phase change of 0.1 rad is of order of 100 μs, which provides information about the time scale available for active phase stabilization. Our results are relevant for future implementations of quantum repeaters in installed optical fiber networks.

DOI: 10.1103/PhysRevA.77.052325 PACS number(s): 03.67.Hk, 42.25.Hz, 42.81.Cn

I. INTRODUCTION

Distributing quantum resources over large distances is an important experimental challenge in quantum information science [1]. One possibility to overcome losses in optical fibers is to implement a quantum-repeater architecture [2] where the total distance is split into several segments. Entanglement between neighboring nodes in each segment is created independently and stored in quantum memories. The entanglement is then extended to longer distances by entanglement swapping.

One way to create entanglement between remote material systems is by quantum interference in the detection of a single photon emitted by the atomic systems [3–9] [see Fig. 1(a)]. The remote atoms are excited in a coherent fashion and the emitted fields are combined at a beam splitter placed at a central location. If the two fields are indistinguishable, the information about the origin of the photon is erased and the detection of a single photon projects the two atomic systems in an entangled state. This type of entanglement creation is probabilistic, but heralded. It has been proposed both for single systems (e.g., single atoms [3,4] or nitrogen-vacancy centers in diamond [6,7]) and for atomic ensembles [5,8]. In the case of ensembles, the creation of entanglement by single photon detection results in entangled number states, with one joint collective atomic excitation delocalized between the remote ensembles, as has been recently demonstrated experimentally [8,9]. The advantage of this type of entanglement is that only one photon must be created, transmitted, and detected, which enables a greater probability per trial to obtain the desired entangled state, as compared to the creation of entanglement by detection of two photons [10–14]. However, the drawback of this method is that it requires interferometric stability over large distances, which is generally considered to be a challenging experimental task. Phase noise in the quantum channels acts as a decoherence in the entanglement generation, in the same way as atomic dephasing acts as a decoherence in the entanglement storage process.

Several solutions have been proposed to alleviate the phase stability problem. (i) First, the two atomic systems can be excited in a Sagnac interferometer configuration [6] [see Fig. 1(b)]. In this way, the excitation lasers for the two memories and the emitted photons travel the same path in a counterpropagating fashion. Hence as long as the phase fluctuations are slower than the travel time, the phase difference is automatically zero. (ii) The second possibility is to stabilize actively the phases, with respect to a reference laser. This requires that the phase fluctuations are not too fast in order to be able to implement a feedback loop [8]. (iii) Finally, a third possible solution has been proposed in [5] for the case of atomic ensembles, by implementing two chains of entangled memories in parallel, with the same quantum channel linking them. In that case, entanglement is generated independently in the two chains, and stored in the memories. By selecting the case where at least one excitation is present in each node, one can obtain an effective two-excitations maximally entangled state. Effective entanglement between remote quantum nodes can thus be created by asynchronous two photon quantum interference [15]. In that case, the phase of the quantum channels must be constant only during the time Δt between the detection heralding the entanglement in the two chains.

While there is an active theoretical activity in developing new quantum-repeaters architectures based on entanglement generation by single photon quantum interference [5–7,16–19], no study has addressed so far the feasibility of the implementation of such protocols in installed telecom networks with respect to phase stability. In this context, we report in this paper measurements of the phase noise in long-fiber interferometers over short time scale. Our results show that the phase in long optical fibers (several tens of km) remains stable at an acceptable level for times of order of 100 μs, in realistic environments.

The measurement of phase noise in optical fibers is also relevant for other applications. There is currently an active area of research aiming at the transmission of frequency references over large distances in optical fibers, in order to synchronize or compare remote optical-frequency atomic clocks [20–24]. In this case, the phase noise in the fiber link directly translates into a spectral broadening of the frequency refer-

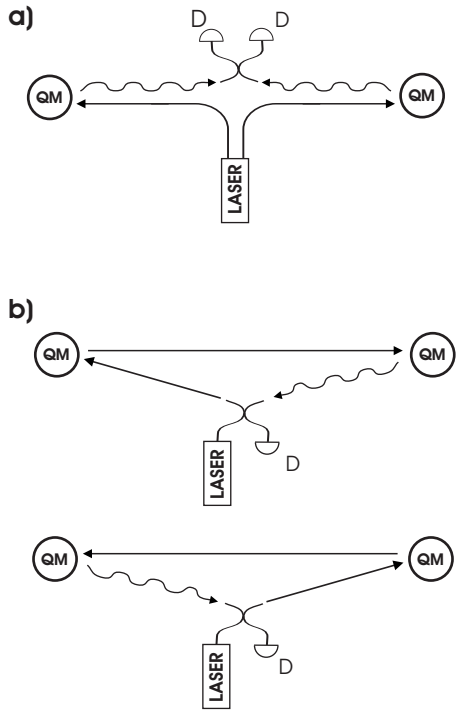

FIG. 1. Creation of entanglement by single photon detection. (a) The two quantum memories (QMs) are placed in the arms of a balanced Mach-Zehnder interferometer and excited with a common laser. The emitted fields are combined at a beam splitter, which erases information about the origin of the emitted photon. The detection of a single photon with detector after the beam-splitter projects the remote QM into an entangled state. In order to generate entanglement, interferometric stability must be preserved for the duration of the experiment. (b) Sagnac configuration. The excitation pulses for each QM are first reflected at the other QM, using, e.g., optical switches. In this way, the excitation lasers for the two systems and the emitted photons travel the same path in a counterpropagating way. Straight lines indicate excitation lasers and wavy lines indicate emitted fields [6].

ence. To preserve the precision of optical clocks, the light should be transmitted with subfemtosecond jitter over long distances through the fiber. Noise cancellation schemes have been developed, which work well as long as the phase noise is negligible during the round trip time of the fiber [23].

In order to perform the phase-noise measurements, we used two interferometric techniques, namely Sagnac and Mach-Zehnder (MZ) interferometry. The Sagnac configuration allows us to study the feasibility of solving the phase stability problem by cancelling the phase fluctuations with the geometry of the interferometer. Moreover, it permits us to visualize the effects of phase fluctuations directly on the visibility of first-order interference, which can then be used as a measure of the fidelity of the quantum communication. However, with this technique we can infer the phase noise only on a time scale shorter than the travel time of the pulses in the interferometer. On the other hand, the MZ interferometer provides some information about the structure of the phase fluctuations over larger time scales. This information is important for the two other proposed techniques to alleviate the phase-noise problem, namely active stabilization and asynchronous two-photon interference. The measurements were performed both in spooled optical fibers in the laboratory, and in installed commercial fibers in an urban environment. The details of the measurements are presented in Secs. II and III and discussed in Sec. IV.

II. SAGNAC INTERFEROMETRY

Information about the phase noise of a long optical fiber can be inferred by measuring first order interference fringes in a Sagnac interferometer. In such an interferometer the two paths correspond to pulses counterpropagating in the same fiber loop. For small distances, the phase in the loop does not have the time to fluctuate during the travel time of the pulses, which leads to a zero phase difference between the two paths of the interferometer. By changing the phase difference between the two pulses (for instance using time resolved phase modulation) it is possible to obtain an interference fringe. If there is no phase noise in the interferometer during the travel time of the pulses, the visibility will be perfect. As mentioned before, this phase fluctuation cancellation technique can be exploited in order to generate remote entanglement of quantum memories by single photon interference. However, for long fibers, the phase might have time to fluctuate during the travel time of the pulses, because the pulses travel through a given segment of the fiber at different times. In that case, the visibility of the interference fringe will be reduced. Hence one can use the visibility as a measure of the phase noise over a time scale shorter than the time of propagation of the light in the interferometer. Let us now investigate in more detail the relation between visibility and phase noise.

Consider that the intensity I at the output of the interferometer is of the form

$$I(\delta\varphi) = \frac{I_0}{2}[1 + \cos(\varphi + \delta\varphi)], \tag{1}$$

where I_0 is the average intensity and φ is a constant phase given by the difference between the two arms of the interferometer. In this model the instantaneous value of intensity I is given by a particular phase fluctuation $\delta\varphi$. Next we assume that the distribution of phase fluctuations reads

$$p(\delta\varphi) = \frac{1}{\sigma\sqrt{2\pi}} e^{-\delta\varphi^2/2\sigma^2}, \tag{2}$$

where σ is the width of the Gaussian distribution. The assumption of a Gaussian distribution of the phase noise will be justified by our results presented in the next section. In order to obtain some characteristic phase-noise independent value $\langle I\rangle$ of intensity, one has to average the intensity described by Eq. (1), such that

$$\langle I\rangle = \int_{-\infty}^{\infty} d\delta\varphi p(\delta\varphi) I(\delta\varphi) = \frac{I_0}{2}(1 + \cos\varphi e^{-\sigma^2/2}). \tag{3}$$

We can thus find a direct relation between the visibility V and the distribution of the phase noise described by σ

$$V = e^{-\sigma^2/2}. \tag{4}$$

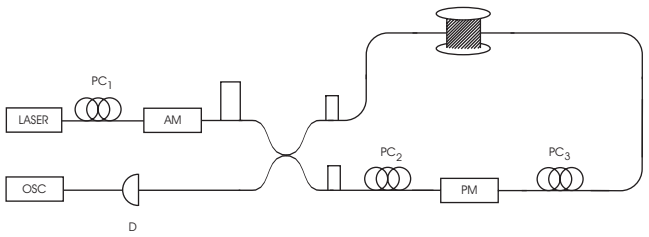

FIG. 2. Sagnac interferometer: experimental setup. A rectangular laser pulse created by amplitude modulator AM is split at the coupler and phase is applied to one of the pulses by the phase modulator PM. The resulting interference signal is detected by detector D and oscilloscope OSC. PC_i denotes polarization controllers.

Let us now describe our experimental setup, shown in Fig. 2. The light source is a single mode distributed feedback laser diode at 1556 nm (linewidth 1 MHz). The light emitted by the laser is modulated by an integrated $LiNbO_3$ optical amplitude modulator (AM) which creates $1-10$ μs rectangular light pulses with repetition rate 1 kHz. These pulses are split at the fiber beam splitter and sent to the Sagnac interferometer. We apply the phase to only one of the pulses by gating a phase modulator (PM) with a pulsed variable voltage. Finally, the interfering light pulses are combined at the fiber beam splitter and the resulting interference signal is detected using a detector and oscilloscope. The area of the pulse is then plotted as a function of the phase shift. The phase is scanned linearly, which results in a sinusoidal interference fringe. The visibility of the fringe is determined by a sinusoidal fit. All the visibilities were obtained after the subtraction of the detector noise from the signal. The phase in the modulator is varied slowly in order to sample the entire Gaussian distribution defined in Eq. (2). The typical time for scanning one fringe is chosen to be about 10 min.

We used several polarization controllers (PC) in order to ensure the optimal polarization alignment. At the same time we made sure that this alignment was quite stable over tens of minutes so that the quick intensity changes are not due to polarization fluctuations. For the experiment in the laboratory conditions, we used spools with different fiber lengths. The spools were inserted in a polystyrene box in order to prevent fast thermal fluctuations. On the other hand, for the measurement in installed fibers, our building is directly connected to the commercial Swisscom network. We had at our disposal two links connecting our building to two different telecom stations in the Geneva area, about 17.5 and 18.25 km away from our building, respectively. Each link was composed of two fibers, connected together at the telecom stations. In this way, we could use two fiber loops of 35 and 36.5 km, respectively, going to different locations. By connecting the two loops together at our building, one can form a 71.5 km long Sagnac interferometer. To connect our laboratory to the telecom network, we used about 150 m of optical fibers.

A typical example of interference fringe is shown in Fig. 3, for the 36.5 km long Sagnac interferometer in installed fibers. One can see that the signal is very stable, even for duration of order of minutes. This is important especially in

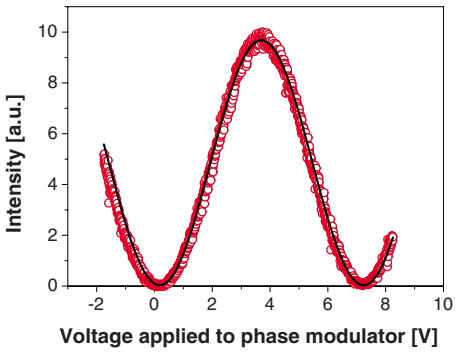

FIG. 3. (Color online) Example of interference fringe for a Sagnac interferometer of 36.5 km in the telecom network. The solid curve is a sinusoidal fit which gives the visibility 99.2%. The time to scan a fringe is about 10 min, which shows that fast phase fluctuations do not degrade the visibility significantly in this case.

the case when one needs to accumulate sufficiently large photon statistics. We investigated the dependence of visibility on the fiber length both in laboratory and real world conditions. The results are shown in Fig. 4. For short distances, the visibility is almost perfect. As expected, a slight decrease of the visibility can be observed when increasing the fiber length, due to phase fluctuations during the travel time of optical pulses. However, the visibilities remain high even for fiber lengths ~75 km. Note that in the 71.5 km interferometer in installed fibers, there is a significant change in visibility for the measurements performed during the day or the night. From the measured fringe visibilities, and attributing all the loss of visibility to phase noise, we are able to express an upper bound for the mean phase change for a given distance using Eq. (4). For instance, for the maximal distance in installed fibers $L=71.5$ km, the measured visibility during the day $V=93.6\%$ corresponds to $\sigma=0.36$ rad and the measured visibility during the night $V=98\%$ corresponds to

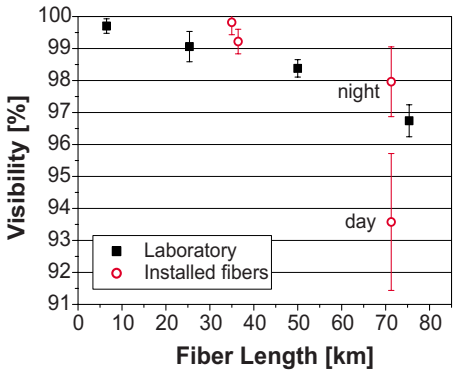

FIG. 4. (Color online) Visibility as a function of fiber length for the Sagnac setup. The decrease of visibility with increasing fiber length is obvious as well as the qualitative agreement between laboratory and telecom measurements. High visibilities confirm the robustness of the Sagnac interferometer setup. For the length 71.5 km, the difference between the day (more phase noise) and night (less phase noise) values of visibilities in the telecom network is worth noting (the night measurements have been performed between 11 p.m. and 1 a.m.). Each point in the graph is the average of a set of interference fringes and the errors are the standard deviations.

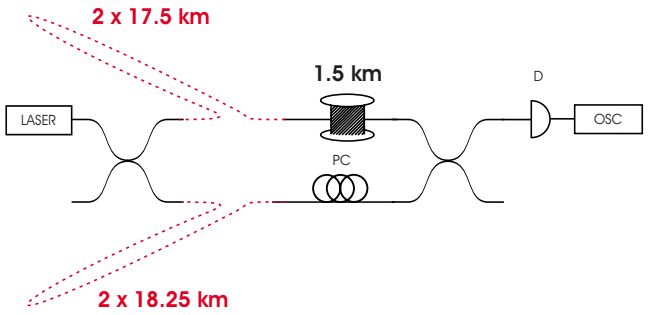

FIG. 5. (Color online) Mach-Zehnder interferometer: experimental setup. Dashed lines denote the telecom fibers. The length difference between the two branches of interferometer was a few cm, i.e., much less than the coherence length of the laser. We used the polarization controller PC in order to optimize the signal at the output. The resulting interference signal is detected by detector D and oscilloscope OSC.

σ=0.2 rad for a travel time 360 μs. One can see that the measurements performed in installed fibers in the urban environment give similar visibilities as those in the laboratory (within the error). The cases where the visibilities in the installed fibers are better than the visibilities expected in the laboratory (25 km interferometer in the laboratory and the 35 and 36.5 km interferometer in the telecom network) might be explained by global vs local disturbance: the long fibers used in laboratory were on spools and when some disturbance such as a mechanical vibration appeared, it was applied simultaneously to the whole length of the fiber whereas in the telecom network such disturbance applied only to the local part of fiber.

III. MACH-ZEHNDER INTERFEROMETRY

As mentioned above, Sagnac interferometry allows us only to obtain information about the integrated phase noise over a time scale shorter than the travel time of a light pulse in the interferometer. In order to obtain a more quantitative analysis over longer time scales, we used Mach-Zehnder interferometry. The experimental setup is shown in Fig. 5. The two arms of the interferometer are composed by the two fiber loops connecting our laboratory to the two telecom stations. In order to balance the lengths of the two arms, we had to add a spool of 1.5 km of fiber in our laboratory. We introduced a polarization controller into one arm of the interferometer in order to align the polarization at the output coupler. Similarly to the experiment with the Sagnac interferometer, we verified that there are no quick intensity changes due to polarization fluctuations. The resulting interference signal is detected by a detector and an oscilloscope with 1 and 6 GHz bandwidth, respectively. We verified that there are no significant changes of light intensity at the detector in the time scale of few μs. It is thus sufficient to use a few datapoints to describe the intensity changes for this time difference without loss of information. In our case the typical distance between two adjacent datapoints was 2–4 μs, which is then the final temporal resolution of the measurement. We also assured that during measurement in this setup the lengths of both arms of the interferometer were equilibrated in such a way that their difference was of order of centimeters. This is much less than the coherence length of the laser (66 m in the optical fiber) corresponding to the measured bandwidth 1 MHz, and leads to negligible phase noise induced by the frequency drift of the laser. In this section we will focus only on measurements performed in the installed fibers.

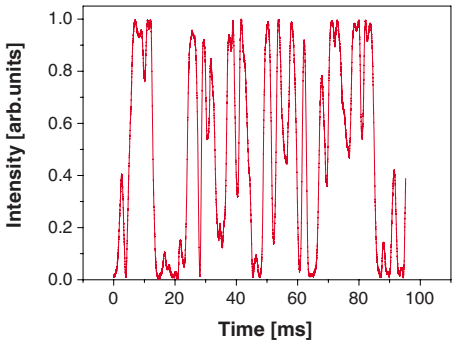

FIG. 6. (Color online) An example of raw measurement of intensity variation as a function of time for the 36.5 km Mach-Zehnder interferometer in the telecom network.

If we consider two interfering light fields, we can find the dependence of measured intensity I on time t in the form

$$I(t) = \frac{I_{\max} - I_{\min}}{2}[1 + \cos\ \varphi(t)] + I_{\min}, \tag{5}$$

where $I_{\max}$ and $I_{\min}$ are maximal and minimal measured intensity and φ is the actual phase difference between the two fields. For our purposes we call from now on this phase difference simply the phase. An example of such a measurement is shown in Fig. 6. From the measurement of $I(t)$ and using Eq. (5) we can directly find the time dependence of the phase. However, around maxima and minima of the signal, a relatively large change in the phase causes only a small change in the intensity and thus introduces a bigger error to the data analysis. On the other hand, on the slope of a measured signal, a relatively small change of phase causes significant change in the intensity. For this reason we restricted our analysis only to this region, omitting maxima and minima; this provides us with less data but should not qualitatively change the obtained statistics. We also verified that the interference is not caused by retroreflections in the interferometer.

Once we calculated the temporal evolution of the phase, we can investigate the phase changes as a function of time. For a time difference τ we can find a set of corresponding phase differences $\{\delta\varphi_\tau^j\}$, where $\delta\varphi_\tau^j = |\varphi(t_j+\tau) - \varphi(t_j)|$, and the final phase difference as the average over j, schematically:

$$\tau : \{\delta\varphi_\tau^1, \delta\varphi_\tau^2, \ldots\} \rightarrow \Delta\varphi_\tau. \tag{6}$$

An example of dependence $\Delta\varphi$ vs τ is shown in Fig. 7. Actually every measurement will give a slightly different (but still monotonously rising) curve, i.e., the times needed for, e.g., a phase change of 0.1 rad will be different. The different measurements are then averaged and statistical er-

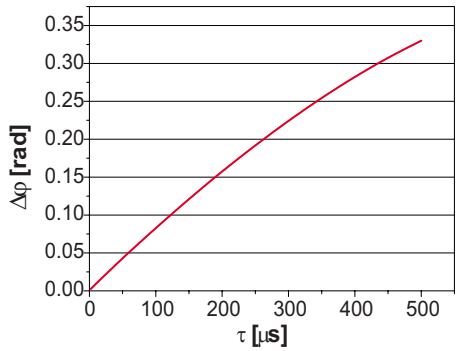

FIG. 7. (Color online) Dependence of the mean phase change $\Delta\varphi$, resulting from the Gaussian distribution (see Fig. 8), on time difference τ as described in Eq. (6). An example for 36.5 km Mach-Zehnder interferometer in the telecom network is shown. Here the time corresponding to the phase change $\Delta\varphi=0.1$ rad is $\tau_{0.1}=122$ μs.

rors can be calculated as shown later in Fig. 9. Another interesting information one can obtain from such a set of phase differences is their distribution. The distribution for a time difference corresponding to the travel time in the interferometer ($\tau=182$ μs) is shown in Fig. 8. In the data processing to obtain this curve, we assume that long terms phase drifts are negligible on this time scale and that the phase fluctuations are random. Thus a positive (negative) intensity change is attributed to a positive (negative) phase change. Hence the $\delta\varphi$ are considered here without absolute value. The Gaussian fit in Fig. 8 shows that the phase-noise distribution corresponds well to a Gaussian distribution. This can be explained if we describe the phase fluctuations in terms of random walk theory [25].

Note that the Gaussian distribution [Eq. (2)] describes fully the phase noise at a given time τ. It is possible to show that there is a direct relationship between this distribution and $\Delta\varphi$ calculated in Eq. (6), such that

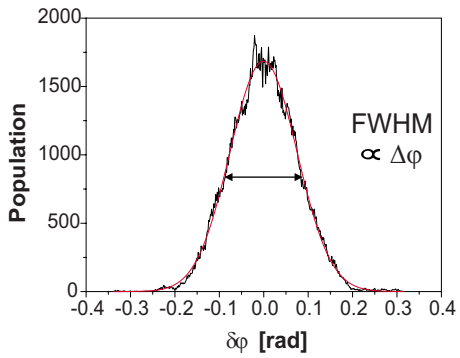

FIG. 8. (Color online) The distribution of the phase noise in the 36.5 km Mach-Zehnder interferometer in the telecom network. The distribution is shown for the time of propagation, i.e., $\tau=182$ μs. One can see that the fit [Gaussian distribution Eq. (2)] corresponds well to the observed results. The average phase change $\Delta\varphi$, plotted in Fig. 7, is proportional to FWHM of the phase-noise distribution.

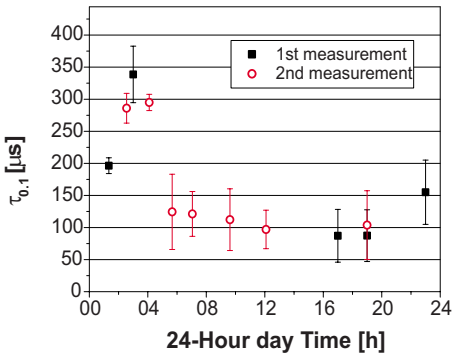

FIG. 9. (Color online) Time intervals needed for phase change 0.1 rad in the 36.5 km Mach-Zehnder interferometer in the telecom network. The first set of measurements consists of points which were measured in the span of 12 days. The second set was obtained during a single day. All measurements are compatible and show the signal with less phase noise during the night (around 3 a.m.) than during the day.

$$\Delta\varphi = \langle|\delta\varphi|\rangle = \sqrt{\frac{2}{\pi}}\sigma. \tag{7}$$

One of the possibilities to quantify the quick phase changes is to fix some value of the phase difference, which can still be tolerated in the mentioned quantum communication protocols and look what is the corresponding time needed for such phase change. We took for example the value of $\Delta\varphi=0.1$ rad, which according to Eq. (4) corresponds to a visibility of 99.5% and we found the corresponding time intervals $\tau_{0.1}$. This value will be further justified in the following section. We investigated how these time intervals changed in installed fibers as a function of the time of day. The results are plotted in Fig. 9. It is obvious that the phase is more disturbed during the day, than during the night, with $\tau_{0.1}$ moving from $\sim$100 μs during the day to $\sim$350 μs during the night. This suggests that a big part of the induced phase noise is due to vibration caused by external disturbances, e.g., traffic.

IV. DISCUSSION

In this section, we discuss in more detail the results obtained with the two interferometric methods. A first interesting point to consider is the dependence of the measured phase noise on fiber length. A common assumption is that the variance of the phase noise var($\delta\varphi$) is proportional to the length of fiber L, where the constant of proportionality is the diffusion coefficient [19],

$$\mathrm{var}(\delta\varphi) = DL. \tag{8}$$

For the measurements in the Sagnac configuration, we can express the diffusion coefficient as a function of the width σ and using Eq. (4) as a function of the visibility V.

$$D = \frac{\mathrm{var}(\delta\varphi)}{L} = \sigma^2\frac{1}{L} = -2\ln(V)\frac{1}{L}. \tag{9}$$

Figure 10 shows the calculated diffusion coefficient as a function of fiber length both for spooled fibers in laboratory

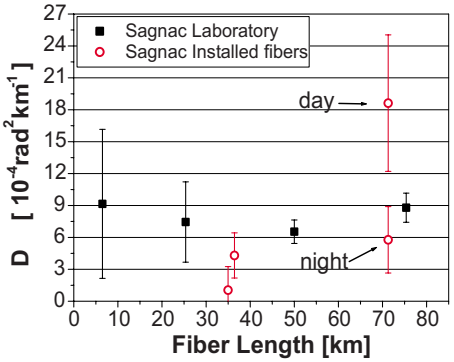

FIG. 10. (Color online) Diffusion coefficients in the laboratory and telecom network. The diffusion coefficients measured in the laboratory yield all the same value (within the error) as expected from theory. For the 71.5 km interferometer in the telecom network, there is, however, a significant difference between the measurements during the day (more phase noise, i.e., larger coefficients) and night.

and for installed fibers. We observe that different fiber lengths yield the similar diffusion coefficient (of order of $D=8\times10^{-4}$ rad^2 km^{-1}). This confirms the assumption that the variance of phase noise is proportional to the fiber length. As expected from Fig. 4, there is, however, a difference for the value of D obtained for the 71.5 km Sagnac interferometer in installed fibers during the day and during the night. This difference might be due to two factors. (i) The phase noise is larger during the day than during the night, as shown in Fig. 9. (ii) In this analysis, all the loss of visibility is attributed to the phase noise, such that the coefficient D is an upper bound. For the 71.5 km interferometer, however, the alignment of polarization was difficult due to a noisy signal. In this case, it is thus likely that a part of the visibility loss is also caused by a polarization mismatch. Note that we do not observe a significant difference between day and night for the Sagnacs interferometers of lengths 35 km and 36.5 km. This might be due to the fact that in this case the whole fiber is in the same cable.

Let us now discuss the results obtained with the Mach-Zehnder interferometer. If we consider the theory of random walk to explain the structure of phase noise, we should obtain a histogram, i.e., a distribution of phase noise in the form of a Gaussian, see Fig. 8. At this point the theory corresponds well to the observed results. The other conclusion arising from random walk theory is that the function plotted in Fig. 7 should depend on τ as τ^x where $x=\frac{1}{2}$. In our case, we find value of x ranging from 0.7 to 0.9. At this point, we do not have a model for the phase fluctuations that explains the observed dependence.

We also considered the effect of a potential slow thermal drift on the observed phase noise. A phase shift of 0.1 rad corresponds to an optical path length difference between the two arms of the interferometer of about 25 nm for a wavelength of 1550 nm. Assuming a drift constant in time (for instance due to a slow temperature variation), an optical path difference of 25 nm in 100 μs would lead to an optical path difference of 90 cm per hour. We measured the optical lengths of the two fibers with a high resolution photon counting optical time domain reflectometer [26], and found that the difference remained constant within a few cm over the course of 12 h (from 1 p.m. to 1 a.m.). This shows that the observed phase noise is most likely due to other causes than a slow thermal drift.

Finally, let us compare the results obtained with the two methods. From the phase noise $\Delta\varphi(\tau=L_{MZ}/c)$ obtained with a Mach-Zehnder interferometer with arm length L_{MZ}, one can predict the visibility one should obtain with a Sagnac interferometer of length $2L_{MZ}$, with the help of Eqs. (4) and (7). In our case the visibility calculated from the Mach-Zehnder interferometer of $L_{MZ}=36.5$ km is $V=(99.0\pm0.7)\%$ during the night (between 11 p.m. and 1 a.m.) and $V=(97.1\pm2.4)\%$ during the day. This is compatible (within the error) with the results for the Sagnac interferometer of 71.5 km shown in Fig. 4.

V. APPLICATIONS TO QUANTUM REPEATERS

Let us now analyze our results with respect to applications in quantum repeaters. As mentioned in the Introduction, there are several ways to alleviate the phase stability problems. The Sagnac configuration presented in Sec. II is very similar to the self-aligned configuration proposed in [6] [See Fig. 1(b)]. In this setup, the two ensembles are excited by a laser pulse traveling in opposite direction in the same fiber loop. In this way, the optical path lengths for the two excitation or emission paths are identical, as long as the phase of the loop is stable for a duration equal to the travel time. Our measurement in urban environment shows that first order interferences with high visibilities can be obtained in such a configuration, for fiber lengths up to 71.5 km (corresponding to a maximal physical distance between the two nodes of 35 and 36.5 km). This shows that from the point of view of phase stability, it is feasible to generate entanglement by single photon quantum interference between two quantum memories separated by tens of km, without active stabilization. Moreover, by using the measurements of the diffusion coefficients (during the night) presented in Fig. 10 and Eq. (9), visibilities higher than 90% can be inferred for fiber lengths of order 250 km.

Alternatively, it is also possible to generate entanglement by single photon detection with a Mach-Zehnder configuration. In that case, however, the phase must be stable for the duration of the experiment, i.e., for a duration several orders of magnitude longer than the typical time of phase fluctuations. Hence in this configuration it is necessary to stabilize the phase actively. Our measurement shows that the phase remains constant at an acceptable level for quantum communication purposes (see below) for duration of order of 100 μs so that the phase noise at frequencies higher than a few tens of kHz can be neglected. Active stabilization at this frequency range seems within reach of current technology (although it remains experimentally challenging). There is currently an active experimental effort to transmit phase references over long distances in optical fibers. In this context, the distribution of a phase reference with subfemtosecond jitter over an actively stabilized fiber link of 32 km length has been recently demonstrated [22].

As mentioned in the Introduction, in order to perform quantum protocols with entangled number states involving one delocalized excitation, one possibility is to implement two chains of entangled memories in parallel and to obtain an effectively entangled state (with two excitations) by post-selection in the final stage [15]. In that case the relevant time scale for phase stability is the time between successful entanglement generations in the two chains. For standard quantum-repeater protocols based on asynchronous two photon interference, Δt can be quite long (orders of seconds), mainly because of the small probability of success per trial and of the limited repetition rate due to the communication time [17]. This means that the phase of the quantum channels should remain stable during this time which is four orders of magnitude longer than the typical phase fluctuation time measured in our experiment (100 μs). Hence in that case, either a self-aligned configuration or an active stabilization are required. However, it is in principle possible to increase by several orders of magnitude the entanglement generation rate with spatial, spectral or temporal multiplexing. For example, in [17], it was suggested that the use of quantum memories allowing the storage of multiple temporal modes (multimode memories) could decrease the required time Δt in order to generate successful entanglement between remote quantum nodes from seconds to tens of microseconds. Our measurement shows that the phase fluctuations on this time scale are acceptable.

Let us finally evaluate how the phase noise propagates in a quantum-repeater architecture and estimate the fidelity that might be obtained with the measured phase noise. In the following analysis for the sake of simplicity we consider only the errors caused by the phase noise. For one elementary link of quantum repeater the ideal state of two entangled memories can be written in the form [17]

$$|\psi_{id}\rangle = \frac{1}{\sqrt{2}}(|01\rangle + e^{i\Phi}|10\rangle), \tag{10}$$

where Φ is the phase difference in between the two arms of the interferometer. If we consider the phase noise in optical fibers, the state for a particular phase shift $\delta\varphi$ is

$$|\psi(\delta\varphi)\rangle = \frac{1}{\sqrt{2}}(|01\rangle + e^{i(\Phi+\delta\varphi)}|10\rangle). \tag{11}$$

For phase shifts $\delta\varphi$ distributed with Gaussian distribution given by Eq. (2), the state of the entangled memories is now given by the density matrix $\hat{\rho}_{real}$

$$\hat{\rho}_{real} = \int d\delta\varphi p(\delta\varphi)|\psi(\delta\varphi)\rangle\langle\psi(\delta\varphi)|. \tag{12}$$

Fidelity can then be calculated from its definition

$$F = \langle\psi_{id}|\hat{\rho}_{real}|\psi_{id}\rangle = \frac{1}{2}(1 + e^{-\sigma^2/2}). \tag{13}$$

The important thing to point out is that if we consider not one but N elementary links and the corresponding entanglement connections [5], the phase shift in Eq. (11) becomes $\delta\varphi = \delta\varphi_1 + \delta\varphi_2 + \cdots + \delta\varphi_N$ and factor σ in Eq. (13) for fidelity becomes $\sigma^2 = \sigma_1^2 + \sigma_2^2 + \cdots + \sigma_N^2$. This is the way the errors add in the considered protocol.

As an example we consider two distant locations separated by 1000 km, connected with eight elementary links [5,17]. We fixed a desired fidelity $F=0.9$ for the entangled state between the two distant places. The fidelity can be also expressed in terms of observed visibility as $F=(1+V)/2$. Using Eq. (4) and the fact that $\sigma^2 \sim L$, we can calculate the allowed mean phase change $\Delta\varphi_{\mathrm{lim}}$ for the 36.5 km segment of fiber. We find $\Delta\varphi_{lim}=0.1$ rad, which motivated our choice of this value in Sec. III. Note that for experimental realizations, other factors will also contribute to the decrease of fidelity, such as dark counts, probability of generating multiple photons, distinguishability between photons, and memory errors.

VI. CONCLUSION

The creation of entanglement between remote quantum memories by single photon interference is attractive for quantum-repeater applications because it is much less sensitive to loss than two-photon schemes, and thus it increases the probability per trial to generate the desired entangled state. This in turns results in shorter times to distribute entanglement over long distances. However, the need for interferometric phase stability over long distances is generally considered problematic from an experimental point of view. In this context, we presented an experimental investigation of phase fluctuations over short time scales in long-fiber interferometers. Our results show that the phase remains stable at an acceptable level for quantum communication protocols for durations of order 100 μs for a 36.5 km long Mach-Zehnder interferometer in installed telecom fibers. This typical time for phase fluctuation should allow an active stabilization of the phase for long interferometers. We also showed experimentally that the phase fluctuations in installed fibers are slow enough to guarantee high visibility first-order interference for Sagnac interferometers over a length of several tens of km, without any active stabilization. This demonstrates the feasibility of observing single photon interference over these lengths, and of its use to generate entanglement between remote quantum memories without active phase stabilization. Our measurements have been performed in installed fibers in a noisy urban environment. An increase in stability is thus expected when using underwater fibers.

ACKNOWLEDGMENTS

We would like to thank M. Legré, D. Stucki, M. Afzelius, and C. W. Chou for useful discussions. We thank Swisscom for giving us access to their optical fiber network. Financial support by the Swiss NCCR Quantum Photonics and by the EU Integrated Project Qubit Applications (QAP) is acknowledged.

[1] N. Gisin and R. Thew, Nat. Photonics **1**, 165 (2007).
[2] H.-J. Briegel, W. Dür, J. I. Cirac, and P. Zoller, Phys. Rev. Lett. **81**, 5932 (1998).
[3] C. Cabrillo, J. I. Cirac, P. Garcia-Fernández, and P. Zoller, Phys. Rev. A **59**, 1025 (1999).
[4] S. Bose, P. L. Knight, M. B. Plenio, and V. Vedral, Phys. Rev. Lett. **83**, 5158 (1999).
[5] L.-M. Duan, M. D. Lukin, J. I. Cirac, and P. Zoller, Nature (London) **414**, 413 (2001).
[6] L. I. Childress, J. M. Taylor, A. S. Sørensen, and M. D. Lukin, Phys. Rev. A **72**, 052330 (2005).
[7] L. Childress, J. M. Taylor, A. S. Sørensen, and M. D. Lukin, Phys. Rev. Lett. **96**, 070504 (2006).
[8] C. W. Chou, H. de Riedmatten, D. Felinto, S. V. Polyakov, S. J. van Enk, and H. J. Kimble, Nature (London) **438**, 828 (2005).
[9] J. Laurat, K. S. Choi, H. Deng, C. W. Chou, and H. J. Kimble, Phys. Rev. Lett. **99**, 180504 (2007).
[10] X.-L. Feng, Z.-M. Zhang, X.-D. Li, S.-Q. Gong, and Z.-Z. Xu, Phys. Rev. Lett. **90**, 217902 (2003).
[11] L. M. Duan and H. J. Kimble, Phys. Rev. Lett. **90**, 253601 (2003).
[12] C. Simon and W. T. M. Irvine, Phys. Rev. Lett. **91**, 110405 (2003).
[13] Z.-B. Chen, B. Zhao, Y.-A. Chen, J. Schmiedmayer, and J.-W. Pan, Phys. Rev. A **76**, 022329 (2007).
[14] D. L. Moehring, P. Maunz, S. Olmschenk, K. C. Younge, D. N. Matsukevich, L.-M. Duan, and C. Monroe, Nature (London) **449**, 68 (2007).
[15] C.-W. Chou, J. Laurat, H. Deng, K. S. Choi, H. de Riedmatten, D. Felinto, and H. J. Kimble, Science **316**, 1316 (2007).
[16] O. A. Collins, S. D. Jenkins, A. Kuzmich, and T. A. B. Kennedy, Phys. Rev. Lett. **98**, 060502 (2007).
[17] C. Simon, H. de Riedmatten, M. Afzelius, N. Sangouard, H. Zbinden, and N. Gisin, Phys. Rev. Lett. **98**, 190503 (2007).
[18] N. Sangouard, C. Simon, J. Minář, H. Zbinden, H. de Riedmatten, and N. Gisin, Phys. Rev. A **76**, 050301(R) (2007).
[19] L. Jiang, J. M. Taylor, and M. D. Lukin, Phys. Rev. A **76**, 012301 (2007).
[20] L. S. Ma, P. Jungner, J. Ye, and J. Hall, Opt. Lett. **19**, 1777 (1994).
[21] I. Coddington *et al.*, Nat. Photonics **1**, 283 (2007).
[22] S. M. Foreman, A. D. Ludlow, M. H. G. de Miranda, J. E. Stalnaker, S. A. Diddams, and J. Ye, Phys. Rev. Lett. **99**, 153601 (2007).
[23] S. M. Foreman, K. W. Holman, D. D. Hudson, D. J. Jones, and J. Ye, Rev. Sci. Instrum. **78**, 021101 (2007).
[24] N. R. Newbury, P. A. Williams, and W. C. Swann, Opt. Lett. **32**, 3056 (2007).
[25] W. Feller, *An Introduction to Probability Theory and Its Applications*, 3rd ed. (John Wiley & Sons, New York, 1970), Vol. I, p. 73.
[26] M. Wegmuller, F. Scholder, and N. Gisin, J. Lightwave Technol. **22**, 390 (2007).